Analysis of the impact of exhaust valve profile on the scavenging and combustion process in a 2-stroke Boosted Uniflow Scavenged Gasoline (BUSDIG) engine

X. Wang, J. Ma and H. Zhao
Centre for Advanced Powertrain and Fuels, Brunel University London, Uxbridge UB8 3PH, United Kingdom.

ABSTRACT:

In order to take advantage of the 2-stroke cycle operation but avoid the drawbacks of conventional ported 2-stroke engine designs, a novel 2-stroke Boosted Uniflow Scavenged Direct Injection Gasoline (BUSDIG) engine was proposed and designed to achieve aggressive engine down-sizing and down-speeding. The uniflow gas scavenging minimises the air short-circuiting through multiple intake ports and exhaust valves in the cylinder head. The intake ports in the BUSDIG engine are integrated to the cylinder liner and designed to create desirable large-scale flow motion. The exhaust valves in the cylinder head are equipped with a variable valve timing actuator and a cam profile switching device. At part-load operation, a low lift exhaust cam profile can be adopted to effectively retain a part of hot residual gas from previous cycle in the cylinder and achieve the hybrid spark ignition (SI) - controlled auto-ignition (CAI) combustion. In order to understand the impact of the low exhaust valve lift profile and the opening timing on the scavenging process and combustion performances, the three-dimensional (3D) computational fluid dynamics (CFD) simulations are performed with a validated SI-CAI hybrid combustion model. It is found that the exhaust valve opening (EVO) timing of the low lift design can be used to effectively control the mass of the trapped residual gas and hence the subsequent scavenging process and intake charge mass. The CAI combustion can be achieved with an appropriate residual gas fraction (RGF) by adjusting the EVO timing. The current work demonstrates the potential of using a low exhaust valve lift design to achieve efficient clean combustion in the 2-stroke BUSDIG engine. The results would be useful for the development of efficient and high power density engines for a range of applications.

ABBREVIATIONS:

3D	three dimensional
AIA	axis inclination angle
aTDC	after top dead center
BUSDIG	boosted uniflow scavenged direct injection gasoline
CAI	controlled auto-ignition
CE	charging efficiency
CFD	computational fluid dynamics
CTR	cross tumble ratio
DI	direct injection
DR	delivery ratio
EL	exhaust valve lift
EVC	exhaust valve closing
EVO	exhaust valve opening
IMEP	indicated mean effective pressure
RGF	residual gas fraction

SD	scavenge port opening duration
SE	scavenging efficiency
SI	spark ignition
SOA	swirl orientation angle
SPC	scavenge port closing
SPO	scavenge port opening
SR	swirl ratio
TDC	top dead center
TE	trapping efficiency
TKE	turbulence kinetic energy
TR	tumble ratio
VVA	variable valve actuation

KEYWORDS:

computational fluid dynamics, 2-stroke engine, uniflow, variable valve actuation, controlled auto-ignition, hybrid combustion

1. INTRODUCTION

The engine downsizing and down-speeding technologies can be used to achieve higher efficiency and reduce the CO_2 emissions from internal combustion engines. However, the application of engine down-sizing and down-speeding by increasing boost is hampered in the 4-stroke gasoline engine due to increased peak cylinder pressure and knocking or low speed preignition (LSPI) combustion. As the 2-stroke engine doubles the firing frequency, it has a lower indicated mean effective pressure (IMEP) and lower peak in-cylinder pressure than a 4-stroke counterpart at the same output. Therefore, the 2-stroke operation can have great potentials to achieve both downsizing and down-speeding. As there is a large overlap between the intake and exhaust processes in the 2-stroke operation, a large amount of hot residual gases can be retained in the cylinder to achieve controlled auto-ignition (CAI) or homogeneous charge compression ignition (HCCI) combustion (1-3). The variable valve actuation (VVA) system can be applied to control the amount of residual gases, as well as the CAI combustion, by adjusting the intake and exhaust valve timings, and the 2-stroke CAI combustion operation can be achieved over a wide range of engine speed and load conditions, including idle operations that could not be achieved with 4-stroke operations (4, 5).

The scavenging process in a 2-stroke engine directly controls the in-cylinder flow motion, charge mixture formation and the subsequent combustion performance. During the 2-stroke scavenging process, the fresh intake charge scavenges the burnt gases out of the cylinder and fills the cylinder for the next cycle. The conventional 2-stroke engines suffer from the fuel/air short-circuiting phenomenon, in which some of the intake fresh mixture would flow directly into the exhaust port during the scavenging process (6), due to the large overlapping period of intake and exhaust process. Compared to the cross and loop scavenge engines, the uniflow scavenged 2-stroke engine shows superior scavenging performance and can operate with little air short-circuiting (7-9). The intake scavenge ports in a uniflow scavenged engine are integrated to the cylinder liner and controlled by the movement of piston top while exhaust valves are placed in the cylinder head. Therefore, the bore distortion caused by uneven thermal loading in the conventional ported 2-stroke engine could be avoided in the uniflow scavenged engine.

In order to overcome the fuel short-circuiting in the conventional 2-stroke engine, the direct fuel injection can be applied after the scavenging process during the intake

and exhaust overlap period (6). However, it was found that the injection timing significantly affects the combustion phase and duration in the 2-stroke CAI operation (10) and the 2-stroke CAI operation modes produce more CO and HC emissions due to the shortened mixing time from the fuel injection to ignition (11, 12). Although the direct injection can avoid the fuel short-circuiting, the air short-circuiting cannot be completely eliminated at high boost pressures because of the overlap period of intake and exhaust processes. The short-circuited air can skew the reading of the lambda sensor in the exhaust, resulting in an enriched in-cylinder air/fuel mixture and hence higher CO and uHC emissions when the exhaust lambda value is set to one (1, 5). Although the stochiometric combustion can be achieved by modulating the fuelling rate or boost pressure, the air short-circuiting would lead to lean mixture in the exhaust and reduce the conversion efficiency of a three-way catalyst (6).

As the exhaust valves are placed in the cylinder head in the uniflow scavenged 2-stroke engine, the variable valve actuation (VVA) technology can be applied to adjust the exhaust valve timings and hence the scavenging process under different boost pressures at various engine speeds. In order to reduce the high CO and HC emissions caused by the insufficient mixing with direct injection (1, 5) and avoid the fuel/air short-circuiting, a low exhaust valve lift was applied in this study to avoid the air/fuel short-circuiting and achieve the CAI combustion with conventional port fuel injection by retaining a part of hot residual gas in a 2-stroke boosted uniflow scavenged direct injection gasoline (BUSDIG) engine (13, 14). In order to clarify the impact of the exhaust valve profiles on the scavenging process and the resultant in-cylinder residual gas fraction and flow motions, the three-dimensional (3D) computational fluid dynamics (CFD) engine simulations with different exhaust valve opening timings (EVO) were performed and analysed in detail at the motored conditions. Then, the combustion processes with different EVO timings were investigated by applying a previously developed spark ignition (SI) - controlled auto-ignition (CAI) hybrid combustion model.

2. SPECIFICATION OF THE BUSDIG ENGINE

The design of the cylinder head, piston shape and scavenge ports of the BUSDIG engine is schematically shown in Figure 1. A pent roof cylinder head was incorporated in the current design to accommodate two exhaust valves, a centrally mounted spark plug and high pressure direct injection (DI) injector. A shallow bowl was included in the piston top to guide the fuel jets from the injector and also to avoid the interference with the spark plug. Twelve evenly distributed scavenge ports were integrated to the cylinder block to introduce the fresh charge and scavenge out the residual burnt gas. Each scavenge port occupies a 20^{o} segment on the cylinder circumference and the interval between two adjacent scavenge ports is fixed at 10^{o}. In terms of the design of the scavenge port, there are mainly four key design parameters, e.g. the axis inclination angle (AIA), swirl orientation angle (SOA), scavenge port opening (SPO) timing and scavenge port height (SPH). As shown in Figure 1, the AIA and SOA were fixed at 90^{o} and 20^{o} respectively in this study, based on the previous study (14). The SPH was kept at 14 mm and the SPO at 130 ^{o}CA. In this study, a low exhaust valve lift (EL) of 3 mm with opening duration of 42 ^{o}CA was applied in order to minimize the overlap between exhaust and intake opening. The exhaust valve opening timing (EVO) were gradually delayed from 84 °CA to 124 °CA after top dead center (aTDC) to study its impact on the scavenging and combustion process. Figure 2 shows the exhaust valve lift profiles and normalized scavenge port opening area profiles. The other engine specifications are shown in Table 1.

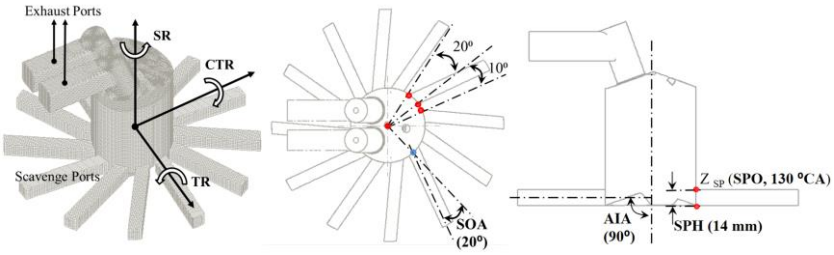

Figure 1. Schematic diagram of the engine design.

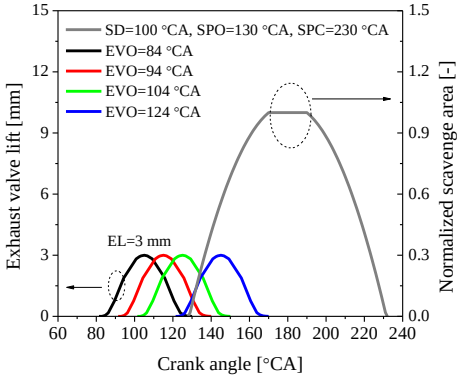

Figure 2. Schematic diagram of the exhaust valve lift profiles and normalized scavenge port opening area profiles.

Table 1. Engine specifications.

Bore	80 mm
Stroke	100 mm
Connecting rod	180 mm
Displacement	0.5 L
Compression ratio	14:1
Cylinder head	Pent roof with 2 exhaust valves, an injector and a spark plug
Piston	Shallow bowl

3. NUMERICAL MODELS

In this study, the simulations were performed with the CFD software STAR-CD (15). The Reynolds-Averaged Navier Stokes (RANS) approach was applied with RNG k-ε turbulence model. The heat transfer was implemented through the general form of the enthalpy conservation equation for the fluid mixture. The Angelberger wall function was used for the simulation of the wall heat transfer.

In order to predict the combustion process in the BUSDIG engine, a set of models for the premixed flame propagation and auto-ignition combustion were employed in this study. The three-zones extended coherent flame model (ECFM3Z), which can consider premixed flame propagation, diffusion flame propagation and auto-ignition combustion, was adopted as the framework of the combustion model. The flame surface density equation was used to describe the flame propagation process and predict the reaction rate of the flame propagation. The average flame surface density is defined as the local area of flame per unit of volume (m^{-1}), which is used to describe the intensity of flame propagation. The tabulated chemistry approach was adopted to predict the auto-ignition of the unburned charge. Chemical kinetic calculations under various thermodynamic and dilution conditions were performed with a reduced gasoline surrogate mechanism (16) to construct the tabulated database of the auto-ignition delay time. The tabulated database is coupled with the CFD simulations by look-up tables. With the tabulated chemistry approach, the auto-ignition tendency was defined to explicitly describe the close degree of fresh mixture from auto-ignition in each cell, and the value of 0 indicates no tendency to auto-ignition and the value of 1 indicates the occurrence of auto-ignition.

During the calculation, the reaction regime of each cell is determined by the average flame surface density and the auto-ignition tendency. The available fuel/air mixture in a cell will be consumed by the flame propagation according to the flame surface density equation when the local average flame surface density of the cell is greater than 0. By contrast, the available fuel/air mixture in a cell will be consumed by auto-ignition combustion according to the tabulated chemistry approach if the auto-ignition tendency of the cell achieves 1. The application of above models enables the prediction of SI combustion, CAI combustion and the SI-CAI hybrid combustion. The detailed modelling and validation of the hybrid combustion basing on the above concept can be found in a previous paper (17).

The ES-ICE software was used to generate the moving mesh for simulations. The arbitrary sliding interface (ASI) was applied between the scavenge ports and the cylinder liner to control the attachment and detachment with the piston movement. The opening and closure of the scavenge ports were determined by the movement of the piston top. ASI was also applied to control the connectivity between exhaust domains and cylinder domain with the movement of exhaust valves. The sensitivity study on the mesh quality showed that an average grid size of 1.6 mm was sufficient to achieve a convergent result (14).

4. SIMULATION CONDITIONS

In order to achieve convergent results, the multi-cycle simulations were applied in this study, and the initial and boundary conditions for the 3-D CFD simulations with motored and fired conditions are shown in Table 2. In the cases with motored conditions, the mixture components for the initial conditions, inlet and outlet boundaries are pure air, i.e. O_2 and N_2. In the cases with fired conditions, the initial mixture components in the cylinder and exhaust ports are pure burned gas, i.e. CO_2, H_2O and N_2, while the initial mixture components in the scavenge ports and the inlet boundary are stoichiometric fuel/air mixtures, i.e. C_8H_{18}, O_2 and N_2. All the simulations were carried out from 60 ºCA after top dead center (aTDC). The crank angle used in this paper is referenced to TDC. The engine speed was fixed at 2000 rpm for all the simulations.

The Pressure-Implicit with Splitting of Operators (PISO) algorithm was used to solve the equations. The equations of momentum, turbulence kinetic energy and turbulence dissipation were discretized with the monotone advection and reconstruction scheme (MARS). The upwind differencing scheme (UD) and central

differencing scheme (CD) were applied to discretize the temperature and density equations, respectively. The residual tolerance for the momentum, turbulence kinetic energy and turbulence dissipation was set at 0.001 while the residual tolerance for pressure and temperature was set at 0.0001 to achieve good compromise between convergence and computational time.

Table 2. Simulation conditions.

	Motored conditions	Fired conditions
Initial conditions		
Cylinder temperature [K]	400	Various (1450 ~ 1540)
Cylinder pressure [bar]	5	Various (9.2 ~ 11.5)
Intake temperature [K]	300	350
Exhaust temperature [K]	400	800
Exhaust pressure [bar]	1.05	1.06
Boundary conditions		
Intake temperature [K]	300	350
Intake pressure [bar]	1.6	1.6
Exhaust temperature [K]	400	800
Exhaust pressure [bar]	1.05	1.06
Cylinder head temperature [K]	340	440
Piston top temperature [K]	360	522
Cylinder liner temperature [K]	320	384

5. RESULTS AND DISCUSSIONS

5.1 Effect of EVO timing on the scavenging process (motored conditions)

Figure 3 shows the effect of the EVO timing on the in-cylinder charge mass. The delayed EVO timing leads to shorter blowdown duration and the exhaust process is significantly weakened as shown in Figure 3. The retained in-cylinder mass would hinder the intake scavenge process and the delayed EVO timing from 84 ºCA to 104 ºCA leads to lower peak intake mass flow rate, as shown in Figure 4. However, the subsequent backflow process offsets the intake process, and the total in-cylinder charge mass at the end of scavenging is similar for EVOs from 84 ºCA to 104 ºCA.
The further delay of the EVO timing to 124 ºCA leads to a distinct scavenging process due to significantly shorter blowdown duration (only 6 ºCA) but longer overlap between the intake and exhaust profiles, as shown in Figure 2. The short blowdown duration leads to only slight decrease of the in-cylinder charge after that the intake fresh charge from the scavenge ports gradually scavenges out the residual gas and fill the cylinder. The overall scavenging process is delayed due to the more trapped residual gas in the cylinder at the early stage of scavenging. As the scavenging proceeds, the increase of scavenging area and exhaust lift leads to stronger scavenging process due to the higher pressure difference between the intake and exhaust, which in turn results in even higher peak intake scavenge flow rate than the earlier EVOs. However, the overall retarded scavenging process and the subsequent backflow leads to lowest in-cylinder charge mass at the end of scavenging, as shown in Figure 3.

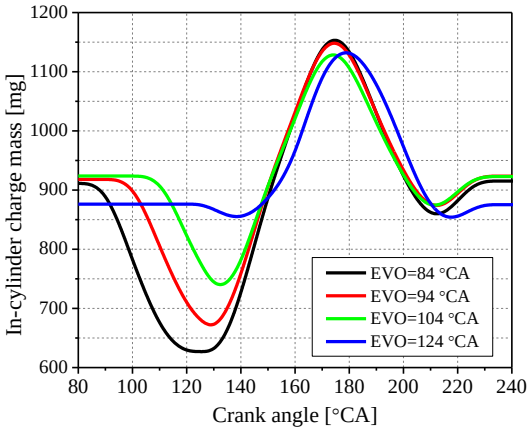

Figure 3. Impact of the EVO timing on the in-cylinder charge mass.

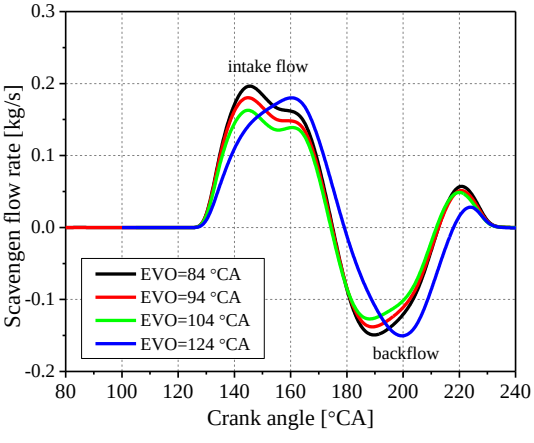

Figure 4. Impact of EVO timing on the intake scavenge flow rate.

In order to understand the impact of the EVO timing on the scavenge process, the in-cylinder residual gas fraction distributions just before the EVC (1st row), after EVC (2nd row) and after IVC (3rd row) for each EVO are shown in Figure 5. As the EVO delays, the incoming fresh charge from the scavenge ports located at the bottom of the cylinder gradually approaches to the exhaust valve just before the EVC. The air short-circuiting is avoided even for the latest EVO timing at 124 ºCA, as there is no air distribution observed in the exhaust ports just before the EVO timing, as shown by the RGF distributions in the first row of Figure 5. However, it is believed that the further delay of EVO timing beyond 124 ºCA would lead to air short-circuiting as there is some air mixture just beneath the exhaust valves before EVC with the EVO timing of 124 ºCA. A large amount of fresh charge starts to fill the cylinder after the closing of exhaust valves and pushes the residual gas to the top of cylinder until the end of the scavenging at IVC.

In order to quantify the scavenging performance, four scavenge parameters, i.e. delivery ratio (DR), trapping efficiency (TE), scavenging efficiency (SE) and charging efficiency (CE), are defined as following:

$$DR = \frac{\text{delivered fresh charge mass}}{\text{reference mass}} \quad (1)$$

$$TE = \frac{\text{mass of delivered fresh charge retained in the cylinder}}{\text{total mass of delivered fresh charge}} = \frac{CE}{DR} \quad (2)$$

$$SE = \frac{\text{mass of delivered fresh charge retained in the cylinder}}{\text{total mass of trapped cylinder charge}} \quad (3)$$

$$CE = \frac{\text{mass of delivered fresh charge retained in the cylinder}}{\text{reference mass}} \quad (4)$$

The reference mass in above equations is calculated by the displaced volume multiplied by the ambient air density.

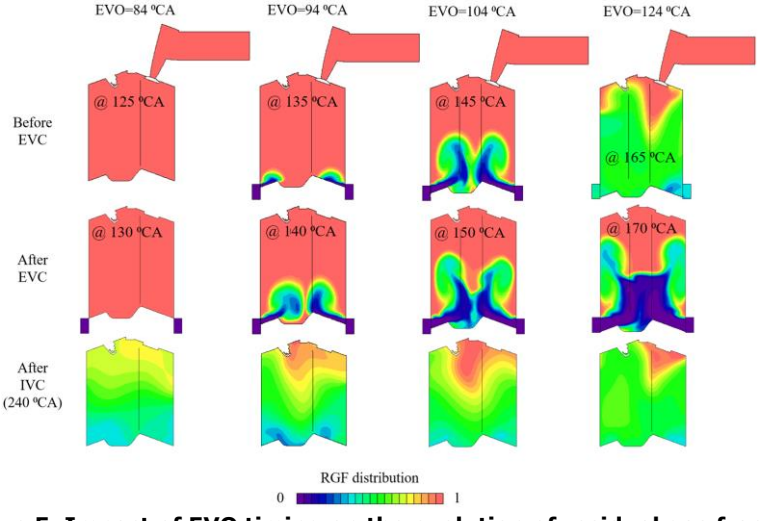

Figure 5. Impact of EVO timing on the evolution of residual gas fraction (RGF) distributions during scavenging.

Figure 6 shows the effect of the EVO timing on delivery ratio (DR), charge efficiency (CE) and scavenge efficiency (SE). As there is no short-circuiting for all EVOs, as indicated in Figure 5, the TE is 1 and DR equals to CE for all cases. As the EVO timing delays from 84 ºCA to 104 ºCA, both DR/CE and SE show monotonous decreasing trends. Specifically, the DR/CE decrease from 0.66 at 84 ºCA to 0.53 at 104 ºCA, and SE from 0.43 to 0.35. The reason can be attributed to the shorter blowdown duration with a delayed EVO timing, which increases the scavenging resistance as more residual gas is trapped in the cylinder during the scavenging process. This then leads to both lower DR/CE and SE.

As the EVO delays to 124 ºCA, the larger overlap between intake and exhaust process leads to enhanced scavenging process of the in-cylinder residual gas, as shown in Figure 4, thanks to the larger pressure differences between intake and exhaust. This in turn leads to slightly higher DR/CE and SE of EVO 124 ºCA than that of EVO 104 ºCA.

The scavenging process also affects the in-cylinder large scale flow motions. The in-cylinder swirl ratio (SR) is defined by the following equation (18):

$$SR(\theta) = \frac{\sum_i^m v_i(\theta) r_i(\theta) V_i(\theta) \rho_i(\theta)}{\frac{2\pi n}{60} \sum_i^m r_i(\theta)^2 V_i(\theta) \rho_i(\theta)} \quad (5)$$

where n is engine speed [rpm], θ the crank angle, i the cell number, $V_i(\theta)$ the cell volume, $\rho_i(\theta)$ the cell density, $v_i(\theta)$ and $r_i(\theta)$ are the tangential velocity and radius respectively in the cylindrical coordinate with z axis as the swirl axis.

Similarly, the tumble ratio (TR) and cross tumble ratio (CTR) are calculated by replacing the Z axis in Equation (1) by the X axis and Y axis, respectively, as illustrated in Figure 1.

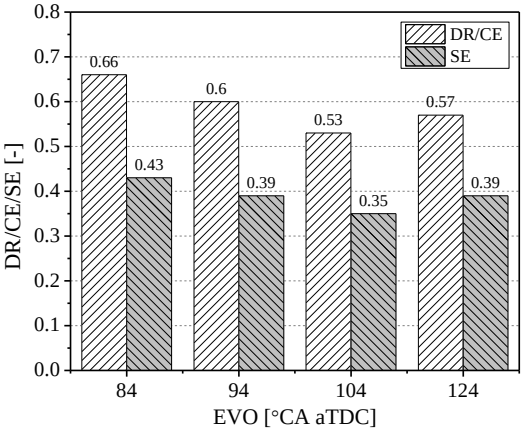

Figure 6. Impact of EVO timing on the delivery ratio (DR), charge efficiency (CE) and scavenge efficiency (SE).

Figure 7 shows the evolutions of the SR, TR and CTR with different EVO timings. The earliest EVO timing of 84 ºCA shows stronger swirl flow motions throughout the cycle. The delay of EVO from 94 ºCA to 124 ºCA leads to lower swirl ratio during and after the scavenging, but produces similar SR level at the top dead center (TDC). In terms of the in-cylinder tumble and cross tumble flow motions, generally they are very weak throughout the cycle, especially around the TDC position due to the substantial decay, for all the EVOs. However, it is still noted the later EVO timing could produce higher peak tumble or cross tumble ratio somewhere during the scavenging, and EVO 104 ºCA obtains highest cross tumble ratio around TDC and EVO 124 ºCA obtains highest tumble ratio around TDC.

Figure 8 and Figure 9 compare the in-cylinder distributions of RGF and turbulence kinetic energy (TKE) respectively for each EVO timing. It is confirmed from Figure 8 that the RGF distribution pattern with more residuals at the top of cylinder persists till the end of compression stroke. The high RGF around the spark plug could affect the initialization and stability of the spark ignitions. Figure 9 indicates that TKE levels for both earliest EVO of 84 ºCA and latest EVO of 124 ºCA are relatively higher than the intermediate EVOs due to their stronger scavenging flow and swirl/tumble flow motions.

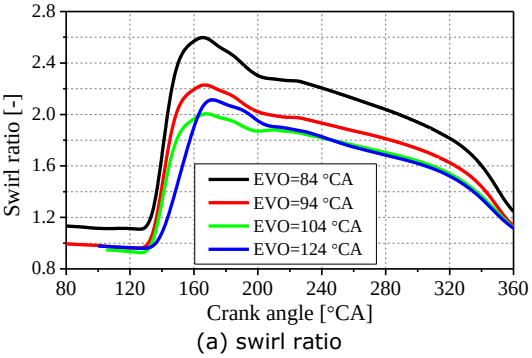

(a) swirl ratio

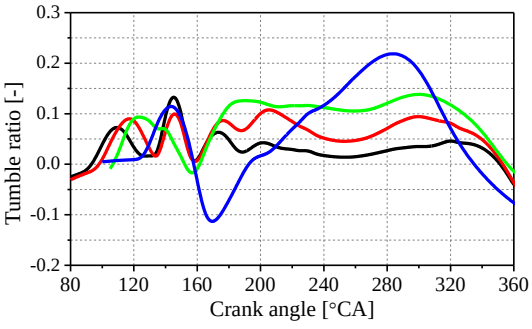

(b) tumble ratio

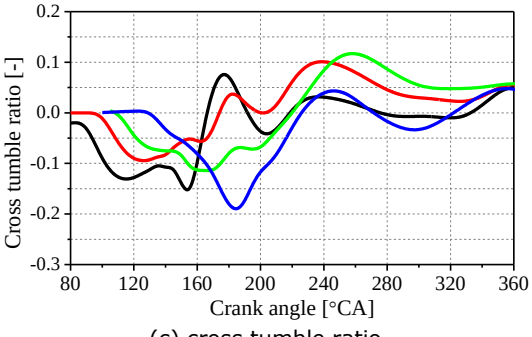

(c) cross tumble ratio

Figure 7. Impact of EVO timing on the in-cylinder (a) swirl ratio, (b) tumble ratio and (c) cross tumble ratio.

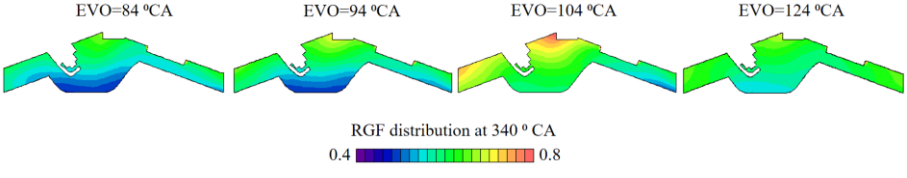

Figure 8. In-cylinder distributions of RGF at 340 ºCA for each EVO timing.

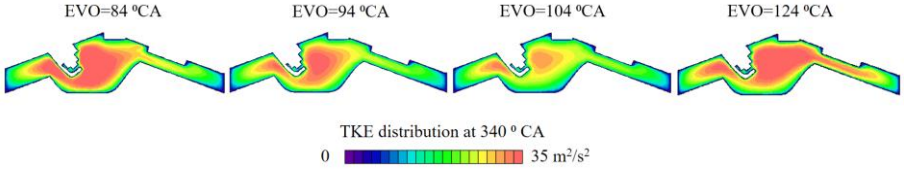

Figure 9. In-cylinder distributions of turbulence kinetic energy (TKE) at 340 ºCA for each EVO timing.

5.2 Effect of EVO timings on the combustion process (fired conditions)

In this section, the combustion models are applied to investigate the impact of EVO timings on the combustion process in the BUSDIG engine. Figure 10 shows the pressure traces of multi-cycle simulations with EVO of 84 ºCA and 104 ºCA. It is

noted that the fired 2-stroke operation simulation is extremely sensitive to the initial conditions and multi-cycle simulations are necessary to obtain the convergent simulation result. In this study, the convergent result can be obtained at the ninth cycle for both EVO of 84 and 104 ºCA. As the EVO timing delays from 84 ºCA to 104 ºCA, the in-cylinder fresh charge is reduced, as indicated by the previous analysis of the scavenging performances, this leads to significantly lower peak in-cylinder pressure from 85 bar with EVO of 84 ºCA to 68 bar with EVO of 104 ºCA. However, it is noted the early EVO timing of 84 ºCA leads to early combustion process and negative work during the compression stroke, producing slightly lower indicated mean effective pressure (IMEP) of 4.1 bar than that of EVO 104 ºCA with 4.2 bar IMEP.

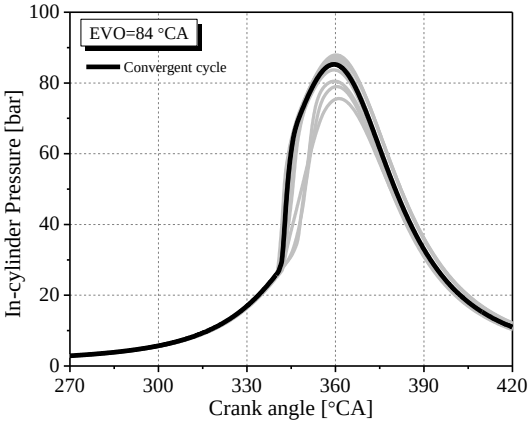

(a) EVO=84 ºCA

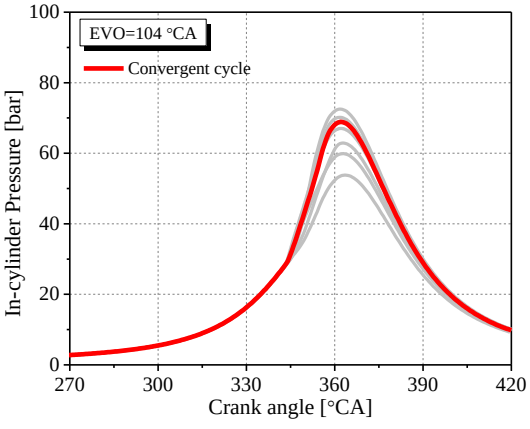

(b) EVO=104 ºCA

Figure 10. Evolutions of in-cylinder pressure traces for (a) EVO=84 ºCA and (b) EVO=104 ºCA.

Figure 11 compares the heat release rate (HRR) profiles with EVO of 84 ºCA and 104 ºCA. In both cases, there is no flame propagation process characterized by a slow heat release rate after the spark timing (340 ºCA), which means the CAI combustion is achieved for both EVO timings of 84 and 104 ºCA. It is noted the auto-ignition occurs right at the spark timing and reaches to its peak value within 5 ºCA and the overall combustion duration is around 10 ºCA. The too-early combustion phasing

leads to significant negative work and reduces the IMEP of EVO 84 ºCA. In comparison, the combustion process with EVO 104 ºCA is much more moderate and commences at around 4 ºCA after spark timing. The subsequent auto-ignition combustion lasts over 20 ºCA, but the main combustion process is completed before TDC, which also deteriorates the IMEP.

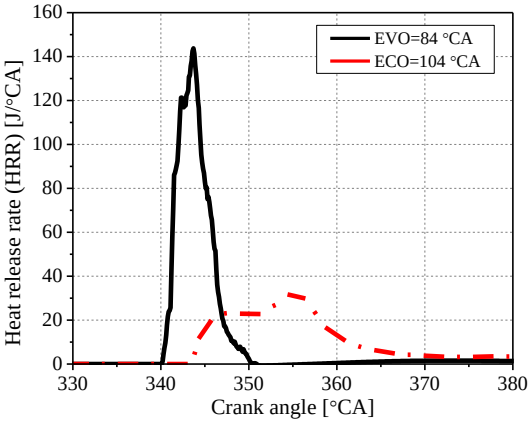

Figure 11. Comparison of the heat release rate (HRR) profiles with EVO of 84 ºCA and 104 ºCA.

In order to understand the different combustion behaviors with EVO 84 and 104 ºCA, Figure 12 compares the average values of RGF, in-cylinder temperature and in-cylinder pressure at 340 ºCA aTDC for each EVO timing. It is noted that the RGF value for late EVO of 104 ºCA is slightly higher, which in turn leads to higher value of in-cylinder temperature. As the overall combustion is much weaker with EVO of 104 ºCA, the average pressure at 340 ºCA is slightly lower. The above analysis of the in-cylinder compositional and thermodynamic conditions indicates that the auto-ignition combustion process is much more sensitive to the dilution effect of in-cylinder residual gas when EVO delays from 84 to 104 ºCA, and the overall more diluted mixture slows down the heat release rate with EVO 104 ºCA although the average temperature is higher.

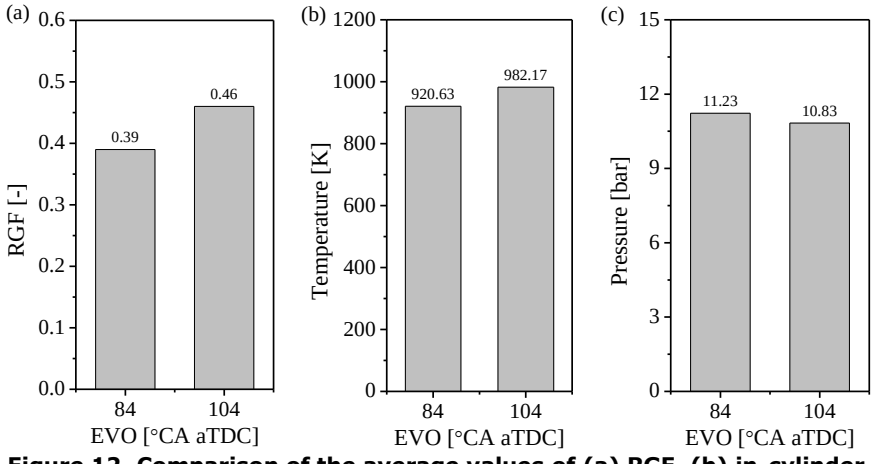

Figure 12. Comparison of the average values of (a) RGF, (b) in-cylinder temperature and (c) in-cylinder pressure at 340 ºCA aTDC with EVO of 84 ºCA and 104 ºCA.

Figure 13 compares the in-cylinder distributions of RGF, temperature and auto-ignition tendency at 340 ºCA for each EVO timing. The high temperature region mainly concentrates in the central region due to less heat transfer loss for each EVO, but the late EVO of 104 ºCA has significantly higher in-cylinder temperature. In comparison, the high RGF region mainly concentrates at the top of cylinder and decreases along the cylinder. It is noted the RGF is extremely higher for late EVO of 104 ºCA that the lowest RGF region at the piston top has slightly higher RGF value than that of the highest RGF region with EVO of 84 ºCA. The over-diluted condition leads to significantly lower auto-ignition tendency, as defined by the close degree of fresh mixture from auto-ignition, in the case with EVO 104 ºCA and the highest auto-ignition tendency appears at the right corner beneath the exhaust valve where the RGF is lowest. In comparison, in the case with EVO of 84 ºCA, the overall auto-ignition tendency is higher and the highest auto-ignition tendency appears at the piston bowl, which also facilitates the propagation of the combustion.

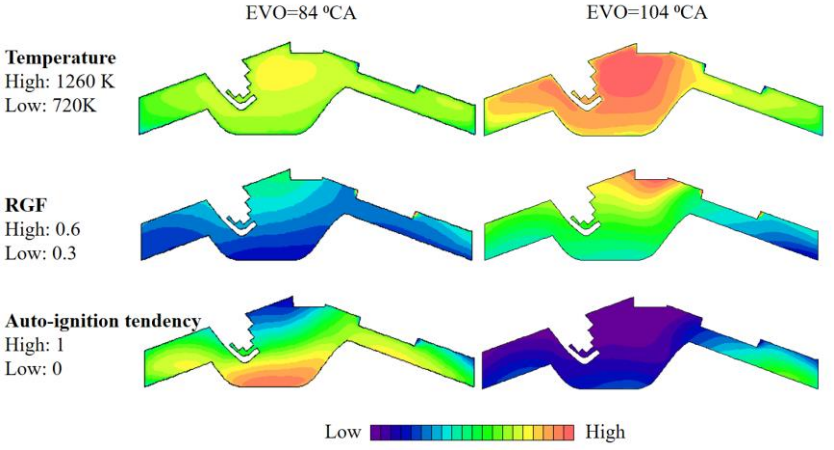

Figure 13. Comparison of the in-cylinder distributions of (a) RGF, (b) temperature and (c) auto-ignition tendency at 340 ºCA aTDC with EVO of 84 ºCA and 104 ºCA.

In this study, the simulation of the combustion process with the later EVO timing of 124 ºCA was also performed. However, it is found the simulation with such a late EVO timing could not achieve the convergence after 9-cycle consecutive simulations. Two distinct combustion modes, i.e. strong combustion and weak combustion cycle, are observed from the pressure traces of the simulation, as shown in Figure 14, and the combustion process jumps between the two modes alternately. Figure 15 shows the intrinsic mechanism of the variations between the strong and weak combustion cycles when applying a late EVO timing of 124 ºCA. A strong combustion cycle produces higher in-cylinder temperature and a large amount of hot residual gas would be retained in the cylinder due to the shorter blowdown duration with a delayed EVO timing. The intake fresh charge for the next cycle is then reduced as a large amount of residual gas occupies the cylinder volume and block the intake charge, which then leads to a weak combustion cycle due to less available fuel/air mixture for combustion. The reduced total in-cylinder charge mass benefits the scavenging process in the next cycle and more intake fresh charge could be retained in the cylinder at the end of scavenging. Then a strong combustion process of more fresh charge can be achieved by either CAI combustion or SI-CAI hybrid combustion thanks to the trapped hot residual gas. The multi-cycle simulations of the combustion process with the late EVO of 124 ºCA indicates that the strong variations of the fresh mixture and

hot residual gas between cycles could produce the potential high cycle-to-cycle variations in the future experimental research.

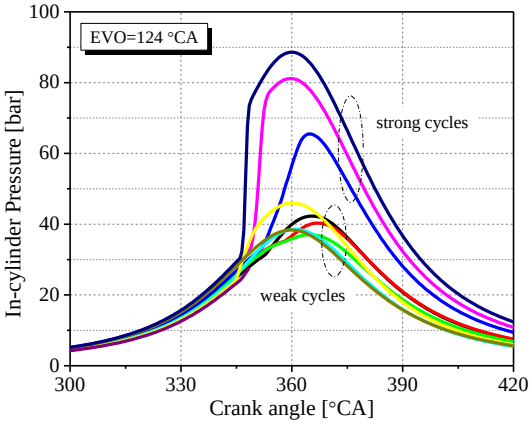

Figure 14. Evolutions of in-cylinder pressure traces with EVO of 124 ºCA.

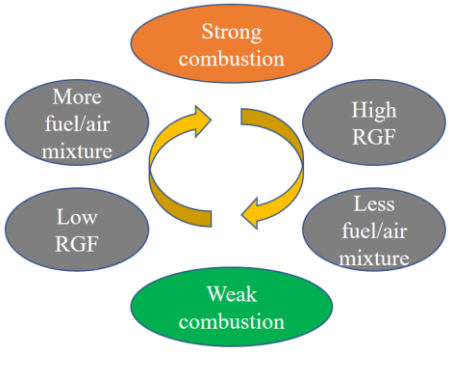

Figure 15. Mechanism of the variation of combustion process with EVO of 124 ºCA.

6. SUMMARY AND CONCLUSION

In this study, the impacts of the low exhaust valve lift profile and the opening timing on the scavenging process and combustion performances in a 2-Stroke Boosted Uniflow Scavenged Gasoline (BUSDIG) engine are investigated by three-dimensional (3D) computational fluid dynamics (CFD) simulations with a validated SI-CAI hybrid combustion model. The main conclusions are summarized as follows:

(1) A low exhaust valve lift profile with a lift of 3 mm and EVO timing ranging from 84 to 124 ºCA was successfully applied in a 2-stroke uniflow scavenged engine to avoid the air/fuel short-circuiting during the scavenging process. The low exhaust valve lift enables the efficient controlled auto-ignition (CAI) combustion to be achieved with premixed fuel/air mixture.

(2) The EVO timing can effectively control the scavenging performances. As there is no short-circuiting for all the studied EVOs, the trapping efficiency (TE) is 1 and the performance of three-way catalyst will not be affected by the presence of excess oxygen. The delivery ratio (DR) and the charge efficiency (CE) gradually decrease from 0.66 at EVO 84 ºCA to 0.53 at EVO 104 ºCA, and scavenge efficiency (SE) from 0.43 to 0.35. The further delay of EVO to 124 ºCA leads to slight increases of DR/CE and SE due to stronger scavenging process with a larger overlap between intake and exhaust process.

(3) The swirl flow motion is strongest for the earlies EVO timing of 84 ºCA. The delayed EVO timing produces higher peak tumble ratio or cross tumble ratio somewhere during the scavenging. EVO 104 ºCA leads to the highest cross tumble ratio around TDC and EVO 124 ºCA results in the highest tumble ratio around TDC.

(4) The complete controlled auto-ignition (CAI) combustion can be achieved with the low exhaust valve lift with EVO timings of 84 ºCA and 104 ºCA. The peak in-cylinder pressure decreases from 85 bar at EVO 84 ºCA to 68 bar at EVO 104 ºCA, and IMEP from 4.1 bar to 4.2 bar. The auto-ignition combustion process becomes much more sensitive to the dilution effect of in-cylinder residual gas when EVO delays from 84 to 104 ºCA. The overall more diluted mixture slows down the heat release rate with EVO 104 ºCA although the average temperature is higher.

(5) The fired 2-stroke operation simulation is found to be extremely sensitive to the initial conditions and multi-cycle simulations are necessary to obtain the convergent simulation result. The combustion process with the latest EVO timing of 124 ºCA alternates between two distinct combustion modes of fast and slow burning, because of large variations of the fresh mixture and hot residual gas between cycles with a later EVO timing.

FUNDING

The authors gratefully acknowledge the financial support by the Engineering and Physical Sciences Research Council (EPSRC). The data of this paper can be accessed from the Brunel University London data archive, figshare at https://doi.org/10.17633/rd.brunel.5371525.v1.

REFERENCE

(1). Zhang, Y., Nora, M.D. and Zhao, H., Comparison of Performance, Efficiency and Emissions between Gasoline and E85 in a Two-Stroke Poppet Valve Engine with Lean Boost CAI Operation. 2015, SAE Technical Paper 2015-01-0827.
(2). Zhang, Y. and Zhao, H., Investigation of combustion, performance and emission characteristics of 2-stroke and 4-stroke spark ignition and CAI/HCCI operations in a DI gasoline. Applied Energy, 2014. 130: p. 244-255.
(3). Zhang, Y. and Zhao, H., Optimisation of boosting strategy for controlled auto-ignition combustion in a four-valve camless gasoline direct injection engine running in two-stroke cycle. International Journal of Engine Research, 2014. 15(7): p. 850-861.
(4). Zhang, Y., et al., CAI combustion of gasoline and its mixture with ethanol in a 2-stroke poppet valve DI gasoline engine. Fuel, 2013. 109: p. 661-668.
(5). Zhang, Y., et al., 2-Stroke CAI combustion operation in a GDI Engine with Poppet Valves. 2012, SAE Technical Paper 2012-01-1118.
(6). Zhang, Y. and Zhao, H., Measurement of short-circuiting and its effect on the controlled autoignition or homogeneous charge compression ignition combustion in a two-stroke poppet valve engine. Proceedings of the Institution of Mechanical Engineers, Part D: Journal of Automobile Engineering, 2012. 226(8): p. 1110-1118.

(7). Abthoff, J., et al., The 2-Stroke DI-Diesel Engine with Common Rail Injection for Passenger Car Application. 1998, SAE Technical Paper 981032.
(8). Laget, O., et al., Preliminary Design of a Two-Stroke Uniflow Diesel Engine for Passenger Car. SAE Int. J. Engines, 2013. 6(1).
(9). Mattarelli, E., Rinaldini, C.A. and Baldini, P., Modeling and Experimental Investigation of a 2-Stroke GDI Engine for Range Extender Applications. 2014, SAE Technical Paper 2014-01-1672.
(10). Zhang, Y., et al., Effects of injection timing on CAI operation in a 2/4-stroke switchable GDI engine. SAE International Journal of Engines, 2011. 5(2011-01-1773): p. 67-75.
(11). Zhang, Y., et al., Experiment and analysis of a direct injection gasoline engine operating with 2-stroke and 4-stroke cycles of spark ignition and controlled auto-ignition combustion. 2011, SAE Technical Paper 2011-01-1774.
(12). Benajes, J., et al., Impact of injection settings operating with the gasoline Partially Premixed Combustion concept in a 2-stroke HSDI compression ignition engine. Applied Energy, 2017. 193: p. 515-530.
(13). Ma, J. and Zhao, H., The Modeling and Design of a Boosted Uniflow Scavenged Direct Injection Gasoline (BUSDIG) Engine. 2015, SAE Technical Paper 2015-01-1970.
(14). Wang, X., Ma, J. and Zhao, H., Evaluations of Scavenge Port Designs for a Boosted Uniflow Scavenged Direct Injection Gasoline (BUSDIG) Engine by 3D CFD Simulations. 2016, SAE Technical Paper 2016-01-1049.
(15). Cd-adapco, Methodology, STAR-CD VERSION 4.14, 2010. 2010.
(16). Mehl, M., et al., An approach for formulating surrogates for gasoline with application towards a reduced surrogate mechanism for CFD engine modeling. Energy & Fuels, 2011. 25(11): p. 5215-5223.
(17). Wang, X., et al., Numerical simulation and validation of SI-CAI hybrid combustion in a CAI/HCCI gasoline engine. Combustion Theory and Modelling, 2013. 17(1): p. 142-166.
(18). Wang, X., Xie, H. and Zhao, H., Computational study of the influence of in-cylinder flow on spark ignition–controlled auto-ignition hybrid combustion in a gasoline engine. International Journal of Engine Research, 2015. 16(5): p. 795-809.